Journal of Intelligent Engineering and Informatics, Vol.1, 2026

Advanced Piezoelectric Single-Crystal Sensors for Underwater Monitoring and Control Systems: Materials, Performance, and Reliability

Dr. S. Vadivazhagi[1,*] S. Lavanya[2]
[1]Professor, Department of Instrumentation and Control Engineering, A.V.C. College of Engineering
[2]Assistant Professor/Dept. of Biomedical Engineering, Jerusalem College of Engineering, Chennai – 600100
Email: vadivazhagiice@avccengg.net

Abstract

Single crystals of relaxor-ferroelectric materials can be used to make compact underwater receivers with excellent electromechanical coupling and piezoelectric response. In deep-sea environments, however, the materials undergo a number of instabilities in domain configuration, pressure-amplified stresses, lack of sensitivity retention, and electrode failure. The survey includes research articles on lead magnesium niobate–lead titanate (PMN–PT), lead indium niobate–lead magnesium niobate–lead titanate (PIN–PMN–PT), doped relaxor crystals, single-crystal composites, domain engineering, and the use of single crystals for hydrophones and vector sensors published between 2015 and 2026. The literature is organized on the basis of crystal chemistry and poling state, connectivity, environmental stabilization, and degree of experimental evidence. The concept of multi-connectivity architectures is new in composite design. Material coupons and water-tank experiments have been studied, showing good hydrostatic figures of merit and wide bandwidth. The main research problem is to realize a field-stable electroacoustic window which exhibits calibrated receiving sensitivity in the presence of coupled pressure–temperature cycling and, at the same time, is appropriate for practical realization in manufacturing.

Keywords: Relaxor ferroelectric; PMN–PT, PIN–PMN–PT, piezoelectric single crystal, hydrophone, underwater acoustics, deep sea, domain engineering, piezocomposite.

I. Introduction

Underwater acoustic receivers need to detect very low dynamic pressures, dissipate heat at low temperatures, withstand salt water, cable loading, long-term unattended operation, and high static pressures. Yet, conventional lead zirconate titanate ceramics still have many uses for the simple reason that they are both cheap and mechanically familiar. Relaxor–$PbTiO_3$ single crystals, particularly PMN–PT and PIN–PMN–PT, introduce a unique design space. Their engineered domains can lead to longitudinal piezoelectric coefficients greater than 1500 pC/N and coupling factors greater than 0.90, thus allowing a smaller active volume to generate a useful electrical signal [1]. High coupling also facilitates the transfer of energy through the composite receiver over a broad band. Based on these benefits, the research topic shifted from material characterization to large-area, curved, vector, and multi-connectivity underwater devices [2]–[7]. These include persistent ocean observation, autonomous platforms, distributed arrays, and sensing at depth. A hydrophone that is sensitive, broadband, pressure-tolerant and repeatable for such applications is required. There has been recent research that has made each of the four ingredients stronger. Rare-earth modification increased the piezoelectric response and boule uniformity [8], [9]; new connectivity concepts resulted in an increased hydrostatic figure of merit and bandwidth [10], [11]; and additive-manufacturing-assisted dice-and-insert routes enabled large composites and curved composites [6], [7], [12] with favorable domain states being produced via alternating-current (AC) poling [13]–[16]. As a result, the number of publications is high; however, this information is distributed across materials journals, the ultrasonics and acoustics journals, sensor journals, and manufacturing journals.

An extensive review of electroacoustic devices [1] shows that relaxor crystals were mostly characterized by intrinsic merit and then segmented by vibration mode and device opportunity. The focus of the latter underwater review was on piezoelectric metamaterials, sound insulation, and energy conversion instead of domain-engineered single-crystal receivers [17]. Both reviews are incomplete, in the sense that they do not go all the way from crystal boule to a calibrated claim for deep-sea sensing. Because this is important to know, a high room-temperature d33 is not necessarily indicative of a high hydrostatic voltage response and a tank result at ambient pressure does not necessarily mean full-

Journal of Intelligent Engineering and Informatics, November 2026, Volume 1, Issue 2, Pages 155-167
Corresponding author. E-mail address: vadivazhagiice@avccengg.net
Received 20 September 2026; **revised** 18 October 2026; **accepted** 15 November 2026; **published** 26 November 2026.
© 2026 Scholarly Horizon Publication. All rights are reserved including those for text and data mining, training of AI and similar technologies. This is an open access article under the Creative Commons Attribution-Non-Commercial International (CC BY-NC 4.0) License

ocean-depth service. Recently, there has been a significant amount of activity in the field of pressure-stable, domain-engineered relaxor single crystals and their composites for broadband passive reception, and yet to date no single, comprehensive survey was found within this precise field of interest. Medical and transmit-only studies were only used if their development or testing approach is usable on receiving devices.

The literature falls within five interconnected areas, namely crystal chemistry and growth, crystallographic cut and domain configuration and poling, monolithic or composite connectivity, pressure–temperature and package stabilization, and evaluation realism. It is not a chronological list but rather a causal taxonomy. It illustrates the point of sensitivity, the point of insensitivity, and the degree of proof in each claim. The specific contribution in the case of the survey is this concept of a field-stable electroacoustic window; a deployable (material + device) combination must remain hydrostatically sensitive with calculated receiving voltage sensitivity and must not be adversely affected by coupled pressure/temperature cycling that would result in unacceptably poor bandwidth, noise performance, production yield, or repairability. There is a need in the future for retained properties, not just initial peaks, to be reported, for domain imaging to be linked to acoustic calibration, and for development to move from finite-element models to pressure chambers and then to sea trials.

The following sections map the boundary, calculate common metrics, compare the architectures, identify deployable methods, and use the evidence gaps as a qualification agenda. This framing avoids three error-prone comparisons. It is to be noted that a free crystal coefficient cannot directly be compared with the sensitivity of a packaged hydrophone. Secondly, bandwidth values cannot be combined if the decibel limit, center frequency, and electrical load are different. Third, a chamber-evaluated pressure rating cannot be shown next to a simulated pressure rating without an evidence label. As a consequence, the original test contexts of the corresponding numerical results are established and the transmitter studies are classified as architecture comparators.

II. Review Scope and Evidence Method

A. Exact Boundaries

The bulk relaxor-ferroelectric single crystals and single-crystal/polymer composites are considered the active receiving elements of an underwater acoustic sensor. The time boundary is January 2015 to 4 August 2026. They include binary crystals of PMN–PT, ternary crystals of PIN–PMN–PT (also abbreviated PIMNT), manganese modifications and rare-earth modifications of relaxor–PT crystals. Examples of included device forms are monolithic plates or bars, 1–3 and 2–2 composites, curved or conformal composites, dual- or multi-connectivity composites, pressure hydrophones, and vector sensors. Unlike the first group, studies of growth, cutting, electrodes, face plates, backing, polymer fill, and pressure mechanics contribute when they impact receiving performance or reliability. The definition of scope for selection is provided in Table 1. These are ceramic-only, biomedical, and projector studies that are not analyzed as direct evidence of hydrophone use. They only manifest themselves when they isolate a transferable manufacturing, mode-control, or bandwidth mechanism. Outside the boundary are thin-film microelectromechanical systems (MEMS), optical and fiber receivers, triboelectric devices, energy harvesters, and non-acoustic ocean sensors. Lead-free materials are mentioned as a future constraint but are not yet a fully developed alternative, as the deep-sea single-crystal receiver papers reviewed to date largely use lead-based relaxor–PT materials.

Table 1. Exact survey boundary and treatment of adjacent literature.

Dimension	Included evidence	Excluded or comparator-only evidence	Reason for boundary
Publication period	Peer-reviewed journal work, 2015–4 August 2026	Earlier work except concepts discussed in the 2015 review [1]	Captures the recent device and pressure-stability wave
Active material	PMN–PT, PIN–PMN–PT/PIMNT, Mn- and rare-earth-modified relaxor–PT single crystals	Polycrystalline ceramic as primary subject	Keeps the review centered on single-crystal development
Device role	Passive hydrophone, vector sensor, receiving characterization	Transmit-only projector as direct performance evidence	Receiving sensitivity is the target claim
Architecture	Monolith, 1–3, 2–2, curved, conformal, and multi-connectivity composites	Thin-film MEMS and non-piezoelectric receivers	Different scaling and failure physics

Environment	Water tank, hydrostatic chamber, pressure/temperature cycling, sea trial	Air-only resonance as deployment proof	Deep-sea reliability requires wet and pressure evidence
Adjacent studies	Fabrication, poling, coefficients, electrode adhesion, transferable bandwidth design	Medical imaging and energy harvesting results as rankings	Transfer mechanisms without mixing application metrics
Evidence requirement	Traceable methods, numerical values or clearly stated observations, valid DOI	Conference abstracts, promotional claims, unverified identifiers	Supports reproducible synthesis

B. Search and Review Methodology

The search was a purposive and structured search and not a statistical meta-analysis. Titles and abstracts were initially filtered for relevance directly. Full records were then checked to obtain data about crystal composition, cut or poling state, connectivity, operating frequency, acoustic medium, reported sensitivity/coupling, environmental load, and digital object identifier (DOI) validity. A paper can have multiple branches of the taxonomy. For instance, hydrophone performance is addressed by the large-area, 3-D-printing-assisted composite study aimed at manufacturing scalability, while package reliability is addressed by electrode comparison without focusing on intrinsic crystal merit. Individually, each experiment was marked on an evidence ladder.

In addition, L0 includes prediction by analysis without the actual fabrication of an active device. Material coupons, impedance spectra, coefficients, and adhesion tests are present in L1. L2 includes calibrated/comparative ambient water-tank measurements. L3 includes hydrostatic-pressure or coupled environmental testing to be followed by post-load electrical or acoustic verification. A sea test of reported duration and depth is included in L4. This ladder restricts language used in the synthesis: operational full-depth survival would require an L0 study to identify a reasonable stress mechanism. Water-coupled response can be achieved with L2 study but pressure retention cannot.

C. Review Novelty: The Field-Stable Electroacoustic Window

The innovative challenge is not to get to a new maximum of one performance factor. Rather it is to determine the co-operative operating area that meets the hydrostatic receiving response, bandwidth, noise floor, domain state, and package integrity criteria given the actual load history experienced in the device. The field-stable electroacoustic window is this area. In this context field-stable is defined as stable in service conditions and not just stability in an applied electric field. The window connects quantities which are typically reported in separate studies and which are evaluated on different operating scales. It also suggests an important qualification issue: while a void might close under pressure and improve stress transfer during loading in the early stages of the test, in the later stages of loading, or at higher pressures, the increased concentration of stress could cause debonding or failure due to interfacial shear. Therefore, initial-performance and performance-retention data need to be obtained under representative pressure–temperature loading cycles.

III. Governing Model and Common Metrics

A. Linear Piezoelectric Relations

For small-signal receiving operation, the strain-charge form relates mechanical stress, electric field, strain, and electric displacement:

$$S=s^{E}T+d^{T}E. \quad (1)$$

$$D=dT+\varepsilon^{T}E. \quad (2)$$

Here, s^{E} is compliance at constant electric field, d is the piezoelectric tensor, and ε^{T} is permittivity at constant stress. Crystallographic cutting and engineered domain state are central here because they rotate the hydrostatic or vector loading effective tensor. They also describe how a polymer matrix can be beneficial. A decrease in composite permittivity may increase the voltage response even when the composite charge coefficient is less than that of the free crystal.

For a transversely symmetric receiver under uniform pressure, hydrostatic charge response is

$$d_{h}=d_{33}+d_{31}+d_{32}\approx d_{33}+2d_{31}. \quad (3)$$

The approximation is valid when $d_{31}=d_{32}$. A large d_{33} alone is not sufficient because the transverse terms usually oppose the longitudinal term. Composite connectivity, cut, and face-plate stress redistribution can reduce cancellation or create an additional useful charge path [6], [10], [11], [18]. Hydrostatic voltage coefficient and hydrostatic figure of merit are

$$g_{\mathrm{h}}=\frac{d_{\mathrm{h}}}{\varepsilon_{33}^{T}}, \qquad F_{\mathrm{h}}=d_{\mathrm{h}}g_{\mathrm{h}}=\frac{d_{\mathrm{h}}^{2}}{\varepsilon_{33}^{T}}. \tag{4}$$

F_{h} is useful for material and composite screening, but it is not a complete sensor metric. A finished hydrophone also contains electrodes, encapsulation, cable capacitance, preamplifier loading, mechanical resonances, and pressure-dependent boundary conditions.

B. Electromechanical Coupling and Response

For longitudinal operation, a common coupling expression is

$$k_{33}^{2}=\frac{d_{33}^{2}}{s_{33}^{E}\varepsilon_{33}^{T}}. \tag{5}$$

High coupling supports efficient conversion and broad matching possibilities, but usable receive bandwidth must be measured on the assembled device. Open-circuit receiving voltage sensitivity (RVS) is written as

$$M_{V}(f)=20\log_{10}\left(\frac{|V_{\mathrm{oc}}(f)|}{p(f)}\right) \quad \text{dB re 1 V/}\mu\text{Pa}. \tag{6}$$

The value of the reference, electrical termination, range, calibration hydrophone, and value of frequency smoothing should be specified. Otherwise, a value without such conditions is not directly comparable. Similarly, bandwidth can refer to a −3 dB or −6 dB bandwidth, a fractional bandwidth, or an impedance bandwidth. The original definition is retained in the review, and no conversion between unlike measures is presented. For instance, it was reported that the 2–2 PIN–PMN–PT hydrophone has a response on the order of 220 kHz, and its −3 dB bandwidth and receiving sensitivity are >55 kHz and >−180 dB re 1 V/μPa, respectively [19]. The immersion transducer constructed with Mn:PIMNT/epoxy 1–3 showed the −6 dB bandwidth of 111.4% [20]. Both show a general response, although the criteria and devices vary.

A. Operational Stability and Reliability

To compare stability studies, this survey defines a dimensionless retention factor for any property X:

$$R_{X}(P,T,N)=\frac{X(P,T,N)}{X(P_{0},T_{0},0)}. \tag{7}$$

P is hydrostatic pressure, T is temperature, and N is the number of pressure, temperature, or electrical cycles. Relevant choices are $X\in\{d_{\mathrm{h}},F_{\mathrm{h}},M_{V},k,\tan\delta\}$. A retention curve is stronger evidence than a pass/fail statement because it shows reversible shifts, permanent loss, and the onset of failure. The field-stable electroacoustic window can then be expressed as the set

$$\Omega_{\mathrm{FS}}=\left\{(P,T,N):R_{M_V}\geq\eta_{M},\ R_{B}\geq\eta_{B},\ R_{\mathrm{ins}}\geq\eta_{I},\ Y\geq\eta_{Y}\right\}, \tag{8}$$

where R_B is bandwidth retention, R_{ins} is insulation or leakage retention, Y is production yield, and the thresholds η are chosen for the mission. This is a survey framework, not a claim that one reviewed device already satisfies all thresholds.

IV. Classification of Single-Crystal Sensor Approaches

A. Crystal Chemistry and Growth Uniformity

Attractive aspects of binary PMN–PT are mature growth and cutting routes and the remarkably high response of its near-morphotropic compositions. The disadvantage is that it has a small coercive field and does not have large thermal margins around the phase transitions. Typically, ternary PIN–PMN–PT (often written PIMNT) has a higher coercive field and a broader usable temperature range and so is a better starting choice for high-drive or variable-temperature service [1]. Manganese modification can be used to reduce dielectric loss and to ensure stable resonant operation; in 2024, the 1–3 Mn:PIMNT/epoxy device with d33 near 1220 pC/N, g33 = 37.87 × 10−3 V m/N, k33 near 0.90 and a broad immersion response was reported [20]. The rare-earth modification involves response and uniformity. Sm-doped PMN–PT crystals exhibited d33 as high as 3400–4100 pC/N with a variation not exceeding 20% [8]. For Nd-doped PMN–PT, the moderately high values of ΔP and d33 of about 3000 pC/N and 16 nm2/N, respectively, were obtained at the rhombohedral to tetragonal transition temperature region of 74 – 87 °C [9].

Although important for miniaturization and sensor-production consistency, neither maximum coefficient alone is an indication of deep-sea stability. An increased permittivity causes a decrease in

gh and a highly mobile domain state is more susceptible to bias, stress, or temperature. Doping must thus be optimized around a device-level retention target. Growth technology is key to scaling lab properties to many sensor elements. Continuous-feeding Bridgman growth is a solution to composition drift and crystal utilization [21]. Composition, phase-transition temperature, dielectric loss, coercive field (Hc), and effective piezoelectric constants (both growth and radial) should be given by boule mapping. For a deep-sea array, it is important to minimize the spread of units because the calibration error adds up from channel to channel. Thus, uniformity of growth is not a secondary materials issue but an uncertainty of the array.

B. Domain Configuration and Poling Techniques

The rhombohedral crystal is typically a four-domain engineered state for [001] poling and gives good longitudinal response. Two-domain configurations, large shear, or transverse coefficients are possible for the [011]-poled state, which is of interest for compact vector receivers. This is shown in the shear-mode vibrator study, which shows how the orientation and dimensions can be adjusted to optimize the acceleration sensing of a vector hydrophone [4]. The compressive PMN-28PT vector sensor subsequently used finite-element method (FEM) optimization of a small, fabricated device in conjunction with measurement of directivity, demonstrating that anisotropy, typical of a single crystal, can be exploited as a sensing function instead of just a weakness to be avoided [5]. Alternating-current poling is an important recent offshoot. One study [13] found d33 to be enhanced by 21% in AC-poled PMN–PT compared with direct-current (DC)-poled PMN–PT. Field amplitude, frequency, and sample thickness were all found to interact when scaling the process to thin PIN–PMN–PT and therefore no recipe could be taken directly from a coupon to a thin composite post [14]. The field history can also be controlled during electrical de-poling and re-poling, providing an opportunity to restore or alter the performance within a device [15].

The concept is expanded in the case of high-temperature AC poling, in which the domain rearrangement is assisted by high temperature and performed at a lower voltage [16]. The real danger is that, despite the initial response of the domain state, it might not be the most stable one when it comes to service stress. Interactions between electrical, thermal, and mechanical histories are illustrated with polarization fatigue in PIN–PMN–PT [22] and combined thermal-mechanical loading [23]. In PMN–PT (also abbreviated PMNT) and PIMNT, the dielectric relaxation processes are also observed, which are frequency- and temperature-dependent and may influence low-frequency noise and calibration [24]. Thus, Table 2 is a comparison of the poling strategies based on the expected value of implementing them, not solely on the maximum coefficient.

Table 2. Material and domain-engineering taxonomy for underwater receivers.

Approach	Main performance lever	Main instability or scale-up risk	Present evidence	Best-fit sensing use
Binary PMN–PT	Remarkably high d_{33} and coupling [1]	Lower coercive and thermal margin; property spread	Extensive coupon and device evidence	Ambient-to-moderate-depth high-sensitivity receiver
Ternary PIN–PMN–PT/PIMNT	Higher field and temperature tolerance [1], [20]	More complex composition control	Coupons, arrays, tanks	Pressure-tolerant broadband hydrophone
Sm- or Nd-modified PMN–PT	Higher response and improved uniformity [8], [9]	High permittivity: domain and temperature stability not yet tied to deep-sea calibration	Material coupons	Miniature arrays after qualification
Mn-modified ternary crystal	Lower loss with strong coupling [25], [20]	Doping–growth trade-off; limited receive pressure data	Prototype transducers, mainly ambient water	Broadband resonant receiver/transceiver
DC engineered domains	Mature, simple production route	May leave less favorable domain population	Broad industrial experience [1]	Production baseline
AC or high-temperature AC poling	Higher d_{33} and controllable domain population [13]–[16]	Thickness scaling, dielectric heating, process-window control	Coupon/composite evidence; limited pressure cycling	High-response posts when in-device verification is possible

C. Conventional Acoustic Receiver Designs

The intrinsic coefficient is maintained and a monolithic crystal plate or bar is quite easy to model but has high acoustic impedance, and lateral constraints reduce hydrostatic response. This also focuses the stress at mounts and electrodes. Modifying part of the active volume with polymer lowers impedance, lowers permittivity, and provides greater control of vibration modes. Crystal posts are laterally exposed to polymer and continuous through the thickness in a 1–3 composite. Alternating the crystal and polymer plates in a 2-2 composite will produce a material that is continuous in two directions. Hydrostatic charge balance, face area, center frequency, kerf width, pressure path, and fabrication yield are factors in choosing the best option. The 2015 PIN–PMN–PT/epoxy 2–2 array reported thickness coupling as 0.86, effective coupling as 0.884 and a 6 dB bandwidth of 127.7% [2]. It is not a passive

deep-sea qualification, but that study is an array/transducer comparator that shows the bandwidth potential for 2–2 single-crystal composites.

The voltage sensitivity achieved in a subsequent investigation of PMN–PT devices was reported to be up to approximately −166 dB and matched rod response to be greater than approximately −176 dB for the 20–40 kHz frequency range [3]. The dedicated 2–2 hydrophone provided methodical evolution between the principle of constituent-tensors and the homogenized 2–2 model [19] and the coefficient derivation of 2024 strengthened the analytical foundation of translating constituent-tensors into a homogenized 2–2 model [26].

D. Scalable Composite Configurations

As area increases, post width decreases, or as surface curves, traditional dice and fill processing becomes challenging. With dice-and-insert processing, 3-D printing can be used to create a prefabricated polymer frame for supporting and spacing the crystal pieces. A nearly 50 × 50 × 5 mm single-crystal composite that was fabricated by this process achieved a hydrostatic figure of merit of approximately 1469×10−15 m²/N, which is approximately 69.4% higher than a ceramic-composite comparison, and included hydrostatic pressure-stability measurements [6]. This is one of the more practical studies to date because it is connected with pressure evidence, the large aperture, and scalable fabrication. This same manufacturing family allowed a thickness coupling value close to 0.86 and a d33 value close to 1550 pC/N to be obtained [7].

A subsequent conformal structure achieved dimensions of 160 × 50 mm, bent to the extent of 162°, thickness coupling of nearly 0.85, and d33 of nearly 1150 pC/N; the measured band range around 292 kHz was about 60 kHz [12]. Compact arrays and vehicle skins are curved giving aperture and packaging options and gradients in kerf opening, electrode strain and hydrostatic stress. There is a lack of long-duration bend-plus-pressure cycling. The electrodes are a silent but lethal component of this branch.

Comparative adhesion testing showed approximately 3.5 MPa for a low-temperature silver paste, 2.1 MPa for sputtered gold and 0.9 MPa for electron-beam-deposited gold on the single-crystal composites studied in this work [27]. Conductivity, corrosion resistance, compliance, process temperature, and bond strength must all be optimized simultaneously. A highly conductive, brittle film can fail at a curved kerf edge and a compliant paste can add thickness and variability. Therefore, it is important to qualify the electrodes on the completed geometry.

E. Connectivity and Stress Management

Recent architectures deliberately create more than one useful piezoelectric charge path. The (1A,1B)-3 composite achieved a separation of two active substructures in a polymer matrix with a hydrostatic figure of merit (HFM) of 4084.9×10−15 m²/N and good transmit/receive performance [10]. The 2026 dual-piezo-charge (1–0)–3 design reported 8088.9×10−15 m²/N, roughly 70% sensitivity enhancement, and a −3 dB bandwidth of 130 kHz [11]. Undoubtedly, they are critical advancements for underwater sensing at ambient pressure as they target the cancellation within dh, not just a higher free-crystal d33. Damaging interfacial shear can be exaggerated by the same geometry that will amplify useful stress.

The full-ocean-depth optimization study created both the static-equilibrium and finite-element models for a face-plated 2–2 composite and displayed the sensitivity–stress trade-off [18]. Its full-depth conclusion is modelling-based and has not been sea-validated or evaluated in a full-pressure chamber. This does not mean the study is not valuable, because it identifies the variables that future experiments must measure: the correlation between increased stiffness of the face-plate, increased stress amplification, increased shear at the face-plate interface, and extent of permanent sensitivity loss.

The complete taxonomy is displayed as an architecture that can be edited in Figure 1. The top row details the material-to-deployment chain. The gates below require every proposed design to provide sensitivity, bandwidth/noise, retention, manufacturing, and proof level. Straight arrows assert causality: a device will not be able to repair an unstable boule by chance—even a good tank reaction will not nullify pressure qualification. The last strip contains the new challenge of the survey.

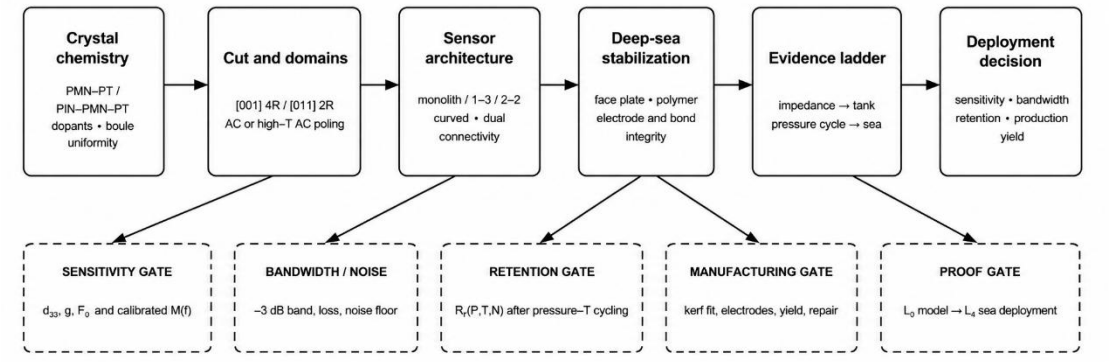


Figure 1. Architecture for pressure-stable domain-engineered single-crystal underwater receivers.

Table 3 condenses the main architecture choices. It separates performance mechanisms from practical limitations and identifies the evidence needed before deployment.

Table 3. Device-architecture classification and implementation trade-offs.

Architecture	Sensitivity/bandwidth mechanism	Practical strength	Main failure or bias	Realistic next proof
Monolithic plate or bar	Preserves intrinsic tensor; cut selects longitudinal or shear mode	Simple electrodes and modelling	High impedance; lateral cancellation; mount stress	Calibrated tank and pressure-cycled $M_V(f)$
1–3 crystal/polymer	Low impedance and permittivity; isolated thickness posts	Broad matching and array compatibility	Kerf damage, post fracture, incomplete fill	Post-level domain check plus pressure retention
2–2 crystal/polymer	Plate connectivity and controlled transverse strain	Manufacturable for large strips; analytical homogenization [19], [26]	Face-plate shear and lateral resonances	Chamber test with interface strain/failure monitoring
Curved/conformal composite	Shapes aperture without rigid backing [7], [12]	Vehicle-skin and compact-array integration	Electrode strain, kerf opening, curvature variation	Combined bending, soak, and pressure cycling
(1A,1B)-3 multi-connectivity	Two active paths improve hydrostatic charge [10]	High F_h with broad response	Assembly tolerance and cross-mode coupling	Batch yield and pressure-cycled calibration
Dual-charge (1–0)–3	Stress redistribution reduces charge cancellation [11]	Highest reported F_h in this evidence set	Complex interfaces; pressure amplification unknown	Independent tank replication and L3 pressure proof
Vector single-crystal sensor	Uses anisotropic shear/compression and directivity [4], [5]	Compact directional sensing	Cross-axis sensitivity and packaging asymmetry	Pressure-dependent vector calibration

The table is read across: no connectivity is universally best, because frequency, aperture, pressure path, and production volume change the optimum.

V. Performance Synthesis by Application and Evaluation Technique

A. Pressure Hydrophones

Pressure hydrophones are designed to be scalar-sensitive to acoustic pressure while rejecting acceleration, cable motion, package effects, and direction. Fh is good as a screening value for this application, but calibrated MVf and equivalent self-noise are more important. New multi-connectivity papers present very high composite Fh figures [10], [11] and large-area/aperture and 2–2 studies provide pathways to practical apertures and calibrated underwater responses [6], [19]. Thus, the highest reported Fh design is not necessarily the best one for the near term. It may be more deployable to use a large, repeatable 1–3 or 2–2 panel with established adhesion of the electrodes and retention in the chamber vs. a complex lab architecture with only ambient tank evidence. Of special interest here are the PMN–PT underwater study [3] and the PIN–PMN–PT 2–2 hydrophone [19] which provide receiving behavior in water.

The dual-charge device introduced in 2026 features an extended testing range [11] and long-term ambient testing [11]. But none of these ambient results is convincing and alone does not solve deep-sea domain and interface stability. Large-area pressure-stability work [6] takes the next step on the ladder of evidence, but a standardized pressure–temperature–acoustic sequence would provide even more evidence for comparison.

B. Vector Sensors

In addition to measuring pressure, vector hydrophones estimate the velocity or acceleration of the particles. Single crystals are helpful as the engineered orientations have increased shear or transverse coefficients. The thickness-shear vibrator analysis [4] is primarily a study of modes and geometry. A

more realistic implementation path was seen in the PMN-28PT compressive vector sensor [5] that progressed to a small prototype sensor, where the directional response was measured. However, hydrostatic load vector calibration continues to be rather limited. Parameters that may vary with static pressure are preload, resonance, cross-axis coupling and package symmetry. A deep-sea vector sensor should therefore be calibrated as a tensor-valued receiver before and after pressure cycling, not as three independent scalar channels.

C. Broadband Acoustic System Comparison

Some included studies target arrays or transducers rather than passive hydrophones, but their architecture evidence is transferable. The 2015 2–2 array study [2] demonstrated high coupling and broad pulse-echo bandwidth. The modelled and fabricated underwater single-crystal composite with an extended usable band reported a 0.83 thickness coupling factor with a broad low reactive power range [28]. The bandwidth of the flextensional design of Mn:PIN–PMN–PT class VII was shown to be 27.8% using finite-element analysis and a prototype, while comparison with PZT as the base model showed that the resulting improvement in transmitting response was 6.3 dB [25]. These results do not directly measure receiving sensitivity but indicate that this sensitivity can be extended through coupling, matching, and the modes of the structure.

AC poling also transfers from material to device. In the case of 1–3 PMN–PT/epoxy composite, d33 increased by 16.41%, ThC increased by 1.97%, the bandwidth increased by 6.27%, and the relative sensitivity by 1.93 dB following AC polarization [29]. A 2–2 composite showed a 36% increase to about 1700 pC/N [30]. These increases are significant because they are obtained in composite forms, but the question of retention remains – does the improved state still remain after dicing, adhesive curing, and pressure, temperature, and time?

D. Protocol-Aware Comparison

The evaluation ladder applied during this survey is shown in Table 4. Each level also indicates the most favorable claim that can be made. The difference is to ensure that a typical wording error is avoided: Designed for full ocean depth does not mean validated at full ocean depth. The 2025 pressure-optimization paper fits the bill for L0 for operational proof as the depth result is analytical and finite-element based [18]. A fabricated ambient tank hydrophone, on the other hand, can be located at L2 even if simulation results are used to support the material coefficients, provided that the locations of workpieces were known.

Table 4. Evaluation realism ladder for single-crystal underwater receivers.

Level	Required evidence	Main quantities	Strongest defensible claim	Typical remaining risk
L0—model	Analytical model or finite-element result	stress, mode, predicted sensitivity	Mechanism is plausible and design is screenable	Material scatter, interfaces, depoling, leakage
L1—coupon/device bench	Fabricated coupon or device; coefficients, impedance, and adhesion in air	d, k, permittivity, loss, impedance, bond strength	Fabrication and small-signal function demonstrated	Water loading and calibration
L2—ambient water	Calibrated or referenced tank measurement	$M_V(f)$, bandwidth, directivity, noise	Underwater response demonstrated at ambient pressure	Static pressure and cycling
L3—environmental chamber	Stated pressure/temperature history plus post-load electrical or acoustic test	R_{M_V}, R_B, leakage, drift, failure count	Qualified for the tested envelope and cycle count	Long duration, handling, real sea variability
L4—sea deployment	Logged depth, duration, reference channel, recovery calibration	in situ drift, self-noise, array consistency	Demonstrated deployment in the stated mission	Broader fleet life and production spread

Representative results, without treating unlike metrics as a league table, are shown in Table 5. It separates claims based on fabrication and evaluation in water from simulation-only depth claims. Values are presented as reported by original papers; blanks represent that the selected metric was not a key finding or part of the study. The causal chain is shown in Figure 1, and the trade-offs and proof limits on Tables 2–5 all indicate the classification of the survey.

Table 5. Representative performance and implementation evidence from 2015–2026.

Study	Material/architecture	Key reported result	Water/pressure evidence	Implementation reading
Yue et al. [2]	PIN–PMN–PT/epoxy 2–2 array	k_t=0.86; 127.7% -6 dB bandwidth	Fabricated array; not a deep-sea receive test	Strong bandwidth comparator
Tian et al. [3]	PMN–PT underwater devices	RVS to about -166 dB; matched rod above -176 dB over 20–40 kHz	Water measurement	Realistic ambient receive evidence

Yeo et al. [5]	PMN-28PT compressive vector sensor	Compact prototype with measured directional patterns	Practical measurements; no deep-pressure proof	Realistic vector prototype
Wang et al. [6]	50 × 50 × 5 mm large-area composite	$F_h \approx 1469\times10^{-15}$ m²/N; 69.4% over ceramic comparison	Hydrophone and pressure-stability evidence	Strongest scale-plus-pressure route in set
Jia et al. [7]	Curved single-crystal composite	$k_t=0.86$; $d_{33}=1550$ pC/N	Fabricated; underwater-transducer oriented	Realistic fabrication, incomplete service proof
Røed et al. [28]	Underwater single-crystal composite	$k_t=0.83$; 132% low-reactive-power band	Model plus fabricated underwater device	Useful broadband architecture comparator
Zheng et al. [25]	Mn:PIN–PMN–PT class VII	27.8% bandwidth and 6.3 dB transmitting voltage response (TVR) gains	Prototype; transmitter metric	Structure transfers; receive ranking does not
Jia et al. [12]	160 × 50 mm conformal composite	162° bend; $k_t=0.85$; 60 kHz band near 292 kHz	Fabricated acoustic transducer	Scalable conformal route; cycling needed
Je et al. [19]	PIN–PMN–PT 2–2 hydrophone	RVS above -180 dB near 220 kHz; >55 kHz -3 dB band	Theory, FEM, and tank experiment	Strong ambient hydrophone evidence
Xu et al. [20]	Mn:PIMNT/epoxy 1–3	$k_{33}=0.90$; 111.4% -6 dB bandwidth	Fabricated immersion device	Broadband realistic prototype
Wang et al. [18]	Face-plated 2–2 full-depth concept	Stress-amplification and interface-shear optimization	Analytical/FEM only for depth claim	Valuable model; simulation-based deployment claim
Lei et al. [10]	(1A,1B)-3 single-crystal composite	$F_h=4084.9\times10^{-15}$ m²/N	Fabricated acoustic tests; no deep-pressure proof	High-performance emerging architecture
Lei et al. [11]	Dual-charge (1–0)–3 composite	$F_h=8088.9\times10^{-15}$ m²/N; 70% sensitivity gain; 130 kHz -3 dB band	Tank and ambient endurance evidence	Highest reported F_h here; L3 validation needed

VI. Environmental Stabilization and Qualification

A. Coupled Environmental and Electrical Effects

Hydrostatic pressure is not only a strength load. It alters the polymer modulus, face-plate contacts, residual stress, resonance, capacitance, and the local field seen by each crystal post. Dielectric and domain dynamics are altered and the polymer is stiffened in cold water. A mechanically biased domain structure can then be acted upon by electrical bias or repolling. If each factor is evaluated individually, the interaction may not be detected. All of these studies—combined thermal-mechanical study [23], polarization-fatigue study [22], dielectric-relaxation study [24], and device-level pressure models [18]—indicate a coupled qualification sequence.

A practical set of measurements starts with room-temperature impedances, capacitances, loss factor of the dielectric, and insulation, dh, and receiving response (calibrated). The device is then soaked; the pressure is raised at a specified rate and maintained at depth-equivalent pressure; the temperature is cycled over the mission range; and the device is returned to the reference conditions. Pressure-based acoustic calibration is repeated whenever possible after pressure recovery and in all cases. There should be a report that includes RX, hysteresis, permanent shift, cycle count, failed units, etc. The fact that one prototype is still in its original condition does not mean one can be produced reliably.

B. Electrode and Encapsulation Design

The active crystal is often stronger electrically than the package is mechanically. Edge flaws may be formed during dicing; residual stress may be present due to polymer curing; electrodes may extend across polymer-crystal interfaces; local peel stress may be present due to the wires; voids may be present in the polymer encapsulation. Each material will compress under pressure in a different way. The electrode comparison [27] indicates that the adhesion due to the deposition method varies significantly, and the full-depth model [18] indicates the influence of the stiffness of a face-plate on increasing the shear stress at the interface. These should be evaluated in combination with representative coupons that contain kerfs, electrodes, bonds, and encapsulation. Monitoring can be non-destructive to improve diagnosis.

Electrical impedance follows mode transitions and changes in bonds. Water intrusion can be detected through insulation and leakage measurements. Voids and debonding can be detected before and after cycling by either acoustic microscopy or X-ray computed tomography analysis. The domain-sensitive image on sacrificial witness pieces can help distinguish depoling from mechanical failures. The aim is not to include all the tests in production but to select those that can easily be measured in the electrical domain and are correlated with acoustic drift at a later point in time.

C. Manufacturing and Calibration Methods

With large-area and conformal routes, production control plays a more crucial role as in [6], [7], and [12]. There are six statistical variables, which are crystal volume fraction, post width, kerf fill, face-plate thickness, curvature, and electrode resistance. Outliers, means, standard deviations, and yield should be provided in batch reports. Derived equivalent coefficients for 2–2 composites [26] could help to create this digital thread from measured components to expected impedances, but the model needs to be modified to include actual part geometry and polymer material properties. Calibration should also correspond to the desired array. This could be due to cable and preamp capacitance. The response of a panel can move when it is acoustically coupled to another panel. For a compact receiver, one might have to integrate the low-noise electronics into the receiver close to the crystal, entailing thermal and pressure-sealing constraints. The final acceptance test should thus be performed on the production termination and housing and not on a bare active stack.

VII. Critical Analysis

In terms of realistic near-term implementations today, conventional 1–3 or 2–2 PIN–PMN–PT/PIMNT composites with controlled dice-and-insert techniques, compliant electrodes and a pressure-qualified face plate are possible. They build on previously identified models of tensors, high coupling, low acoustic impedances, and fabricated evidence from water-tank studies [6], [7], [19], [20], [26]. The 50 × 50 mm pressure-tested composite [6] particularly appears to hold water as it took into consideration the examination of material benefit, manufacturing scale, and environmental behavior in one. Curved and conformal structures [7], [12] are also practically possible, but evidence of electrode strain and bend-plus-pressure fatigue is still required. In this context, the response can be increased by means of AC and high-temperature AC poling [13]–[16], [29], [30].

They are realistic if field uniformity, thickness scaling, heating, and post-process verification are controlled. Rare-earth-modified crystals [8], [9] are promising, but their large room-condition coefficients are not sufficient indicators of hydrophone performance until gh, loss, self-noise, and pressure retention are measured. Multi-connectivity designs [10], [11] have the best reported hydrostatic figures of merit of the designs reviewed and are realistic ambient-water prototypes. They pose a greater risk for immediate deep deployment, owing to their additional interfaces and stress paths. The most well-defined case is the full-ocean-depth optimization [18]. Analytical and finite-element treatments suggest sensitivity amplification and interfacial shear but not survival or calibrated sensitivity at full pressure.

Shear-vibrator optimization [4] is also primarily used as a design basis until packaged pressure tests are introduced. The transmitter bandwidth gain is a useful engineering comparator; it is not a passive-sensor ranking. In the field, d33, Fh, RVS, coupling and bandwidth are measured under various boundary conditions. In order to permit a fair comparison, evidence chains are therefore preferable to record values in isolation. Before depth qualification and performance rank comparisons are made, independent replication of tests across different units should be done. Unlike the coefficient of the largest coupon, it is not the first or largest architecture that will win, but the one that maintains its calibrated response following cycling and which can be built over and over.

VIII. Open Challenges & Future Directions

Sharing a deep-sea qualification protocol is the first priority. This should include a pressure ramp, a dwell, the temperature, the number of cycles, how the device is terminated electrically, what hydrophone it is referenced to, a pre/during/post calibration, and the statistics of RMV failures. Second, the evolution of domains must be associated with the drift of devices. Impedance (in situ) combined with post-cycle domain imaging can be used to rule out reversible changes in boundary conditions from depoling/cracking. Finally, multi-connectivity composites require interface-aware design, treating Fh, shear, leakage, yield, and repairability as interfaces to be optimized, rather than in isolation. Finally, a large number of pressure-dependent cross-axis and phase calibrations are needed for vector sensors. Manufacturing research needs to relate boule location, poling uniformity, kerf fill, electrode resistance to uncertainty in the unit. Physics-based models can then be used directly as digital acceptance tools, not idealized design plots. They must all share the test article: low-noise electronics, cable capacitance, corrosion, biofouling, and long-term water ingress. The lead levels introduce an additional strategic risk; it would be better to benchmark the retained voltage sensitivity and stability, as well as d33, of the lead-reduced or lead-free single crystals. Open datasets should include raw impedance data, chamber history, bad specimens, and recovered device data for independent comparison to the stated limits. A

future L1-to-L3 setup with L4 sea-deployment calibration is the statistically significant separating experiment.

IX. Conclusion

The relaxor ferroelectric single crystals and composites have been found to shift underwater sensing beyond merely coefficient improvement. Now, domain engineering, ternary and doped chemistries, scalable dice-and-insert fabrication, conformal apertures, and multi-connectivity stress paths deliver high coupling and a wide response, along with large hydrostatic figures of merit. However, the quality of evidence is lagging behind, with many devices still only verified by an impedance or ambient water test and full-depth claims that may still be model-based. This survey presents the addition of a causal taxonomy and the field-stable electroacoustic window (comprising sensitivity, bandwidth, pressure–temperature retention, manufacturability, and validation level). It offers an evidence-informed qualification trajectory. The moral is straightforward: do not look at just a room value; be ready for the deep sea with a calibrated receiving response retained after cycling and repeatable production.

References

[1] S. Zhang, F. Li, X. Jiang, J. Kim, J. Luo, and X. Geng, "Advantages and challenges of relaxor-$PbTiO_3$ ferroelectric crystals for electroacoustic transducers—A review," Prog. Mater. Sci., vol. 68, pp. 1–66, 2015, doi: 10.1016/j.pmatsci.2014.10.002.

[2] Q. Yue, D. Liu, J. Deng, X. Zhao, D. Lin, W. Di, X. Li, W. Wang, X. Wang, and H. Luo, "Design and fabrication of relaxor-ferroelectric single crystal PIN–PMN–PT/epoxy 2–2 composite based array transducer," *Sens. Actuators A, Phys.*, vol. 234, pp. 34–42, 2015, doi: 10.1016/j.sna.2015.08.017.

[3] F. Tian, Y. Liu, R. Ma, F. Li, Z. Xu, and Y. Yang, "Properties of PMN-PT single crystal piezoelectric material and its application in underwater acoustic transducer," *Appl. Acoust.*, vol. 175, Art. no. 107827, 2021, doi: 10.1016/j.apacoust.2020.107827.

[4] J. Kim, S. Pyo, and Y. Roh, "Analysis of a thickness-shear mode vibrator for the accelerometer in vector hydrophones," *Sens. Actuators A, Phys.*, vol. 266, pp. 9–14, 2017, doi: 10.1016/j.sna.2017.09.007.

[5] H. G. Yeo, J. Choi, C. Jin, S. Pyo, Y. Roh, and H. Choi, "The design and optimization of a compressive-type vector sensor utilizing a PMN-28PT piezoelectric single-crystal," *Sensors*, vol. 19, no. 23, Art. no. 5155, 2019, doi: 10.3390/s19235155.

[6] T. Wang, X. Zhao, H. Du, S. Xia, G. Li, H. Guo, F. Li, and Z. Xu, "Large-area piezoelectric single crystal composites via 3-D-printing-assisted dice-and-insert technology for hydrophone applications," *IEEE Trans. Ultrason., Ferroelectr., Freq. Control*, vol. 68, no. 10, pp. 3241–3248, 2021, doi: 10.1109/TUFFC.2021.3085842.

[7] N. Jia *et al.*, "High-performance curved piezoelectric single-crystal composites via 3D-printing-assisted dice and insert technology for underwater acoustic transducer applications," *ACS Appl. Mater. Interfaces*, vol. 14, no. 6, pp. 8137–8145, 2022, doi: 10.1021/acsami.1c21010.

[8] F. Li et al., "Giant piezoelectricity of Sm-doped $Pb(Mg_{1/3}Nb_{2/3})O_3$–$PbTiO_3$ single crystals," *Science*, vol. 364, no. 6437, pp. 264–268, 2019, doi: 10.1126/science.aaw2781.

[9] Q. Li, Y. Liu, J. Liu, K. Song, H. Guo, F. Li, and Z. Xu, "Enhanced piezoelectric properties and improved property uniformity in Nd-doped PMN–PT relaxor ferroelectric single crystals," *Adv. Funct. Mater.*, vol. 32, no. 25, Art. no. 2201719, 2022, doi: 10.1002/adfm.202201719.

[10] Y. Lei *et al.*, "A high-sensitivity, broadband (1A,1B)-3 single-crystal composite ultrasonic transducer," *Adv. Funct. Mater.*, vol. 35, no. 11, Art. no. 2417084, 2025, doi: 10.1002/adfm.202417084.

[11] Y. Lei, X. Li, Z. Hou, B. Wang, S. Zheng, Y. Wei, Z. Yu, J. Hong, and S. Dong, "Dual-piezo-charge strategy in (1–0)–3 single-crystal composite for enhancing underwater acoustic sensing," *Nano-Micro Lett.*, vol. 18, Art. no. 259, 2026, doi: 10.1007/s40820-026-02102-1.

[12] N. Jia, T. Wang, L. Ning, Z. Ma, Y. Dang, C. C. Li, H. Du, F. Li, and Z. Xu, "Conformally large-area single-crystal piezocomposites with high performance for acoustic transducers," *ACS Appl. Mater. Interfaces*, vol. 15, no. 30, pp. 36611–36619, 2023, doi: 10.1021/acsami.3c07673.

[13] W.-Y. Chang, C.-C. Chung, C. Luo, T. Kim, Y. Yamashita, J. L. Jones, and X. Jiang, "Dielectric and piezoelectric properties of $0.7Pb(Mg_{1/3}Nb_{2/3})O_3–0.3PbTiO_3$ single crystal poled using alternating current," *Mater. Res. Lett.*, vol. 6, no. 10, pp. 537–544, 2018, doi: 10.1080/21663831.2018.1498812.

[14] H.-P. Kim, H. Wan, X. Lu, Y. Yamashita, and X. Jiang, "Scaling effects in the alternating-current poling of thin PIN-PMN-PT single crystals," *Appl. Phys. Lett.*, vol. 120, no. 14, Art. no. 142901, 2022, doi: 10.1063/5.0084994.

[15] H.-P. Kim *et al.*, "Electrical de-poling and re-poling of relaxor-$PbTiO_3$ piezoelectric single crystals without heat treatment," *Nat. Commun.*, vol. 15, Art. no. 6420, 2024, doi: 10.1038/s41467-024-50847-3.

[16] J.-W. Sun, T. T. Zate, W.-J. Choi, G.-J. Lee, Y. S. Jeong, S.-G. Lee, J. E. Ryu, and W. Jo, "Suppressing phase transformation-induced depolarization in PMN-PT single crystals through high-temperature AC poling," *Scripta Mater.*, vol. 258, Art. no. 116519, 2025, doi: 10.1016/j.scriptamat.2024.116519.

[17] J. Zhao, N. Hu, J. Wu, W. Li, Z. Zhu, M. Wang, Y. Zheng, and H. Dai, "A review of piezoelectric metamaterials for underwater equipment," Front. Phys., vol. 10, Art. no. 1068838, 2022, doi: 10.3389/fphy.2022.1068838.

[18] C. Wang, T. Zhou, R. Ye, X. Yin, and W. Cao, "Performance optimization of piezocomposites-based hydrophone for full ocean depth applications," *Sens. Actuators A, Phys.*, vol. 393, Art. no. 116830, 2025, doi: 10.1016/j.sna.2025.116830.

[19] Y. Je, M. Sim, Y. Cho, S.-G. Lee, and H.-S. Seo, "Theoretical and experimental studies on sensitivity and bandwidth of thickness-mode driving hydrophone utilizing a 2-2 piezoelectric single crystal composite," *Sensors*, vol. 23, no. 7, Art. no. 3445, 2023, doi: 10.3390/s23073445.

[20] Y. Xu, K. Zhu, E. Sun, J. Ma, Y. Li, H. Zheng, R. Zhang, B. Yang, and W. Cao, "Wide-bandwidth immersion ultrasound transducer made of Mn:PIMNT single crystal/epoxy 1–3 composite," *Sens. Actuators A, Phys.*, vol. 369, Art. no. 115196, 2024, doi: 10.1016/j.sna.2024.115196.

[21] K. Echizenya, K. Nakamura, and K. Mizuno, "PMN-PT and PIN-PMN-PT single crystals grown by continuous-feeding Bridgman method," *J. Cryst. Growth*, vol. 531, Art. no. 125364, 2020, doi: 10.1016/j.jcrysgro.2019.125364.

[22] Y. Zhou, Q. Li, F. Zhuo, C. Xu, Q. Yan, Y. Zhang, and X. Chu, "Domain switching and polarization fatigue in rhombohedral PIN-PMN-PT and Mn-doped PIN-PMN-PT single crystals," *J. Am. Ceram. Soc.*, vol. 102, no. 11, pp. 6668–6679, 2019, doi: 10.1111/jace.16461.

[23] F. H. Schader, G. A. Rossetti, Jr., J. Luo, and K. G. Webber, "Piezoelectric and ferroelectric properties of <001>C $Pb(In_{1/2}Nb_{1/2})O_3–Pb(Mg_{1/3}Nb_{2/3})O_3–PbTiO_3$ single crystals under combined thermal and mechanical loading," *Acta Mater.*, vol. 126, pp. 174–181, 2017, doi: 10.1016/j.actamat.2016.12.051.

[24] K. Li, E. Sun, X. Qi, B. Yang, J. Liu, and W. Cao, "Dielectric relaxation and local domain structures of ferroelectric PIMNT and PMNT single crystals," *J. Am. Ceram. Soc.*, vol. 103, no. 3, pp. 1744–1754, 2020, doi: 10.1111/jace.16849.

[25] J. Zheng, S. Li, and B. Wang, "Design and analysis of a broadband class VII flextensional transducer with the third-generation crystal, Mn:PIN-PMN-PT," *Sens. Actuators A, Phys.*, vol. 345, Art. no. 113777, 2022, doi: 10.1016/j.sna.2022.113777.

[26] M. Sim, Y. Je, Y. Cho, H.-S. Seo, and M.-J. Kim, "Derivation of equivalent material coefficients of 2-2 piezoelectric single crystal composite," *Micromachines*, vol. 15, no. 7, Art. no. 917, 2024, doi: 10.3390/mi15070917.

[27] N. Jia, T. Wang, L. Ning, Y. Wang, Y. Dang, Z. Ma, H. Du, F. Li, and Z. Xu, "Comparing different electrodes of piezoelectric single crystal composites for underwater acoustic transducers," *ACS Appl. Electron. Mater.*, vol. 5, no. 1, pp. 350–356, 2023, doi: 10.1021/acsaelm.2c01366.

[28] E. S. Røed, M. Bring, M. Frijlink, A. Henriksen, F. Tichy, E.-M. Åsjord, and L. Hoff, "Underwater single crystal piezocomposite transducer with extended usable frequency band," *Ultrasonics*, vol. 125, Art. no. 106794, 2022, doi: 10.1016/j.ultras.2022.106794.

[29] H. Hang, X. Jiang, D. Lin, F. Wang, X. Wang, and H. Luo, "Performance enhancements of $Pb(Mg_{1/3}Nb_{2/3})O_3–xPbTiO_3$ single crystal/epoxy 1–3 composite by alternating current polarization," *Curr. Appl. Phys.*, vol. 47, pp. 1–8, 2023, doi: 10.1016/j.cap.2022.12.009.

[30] Z. Ma, N. Jia, C. Li, L. Ning, Y. Dang, H. Du, F. Li, and Z. Xu, “Improved piezoelectric properties of 2–2 piezoelectric single crystal composites for acoustic transducer applications via alternating current polarization,” *Mater. Lett.*, vol. 353, Art. no. 135284, 2023, doi: 10.1016/j.matlet.2023.135284.

© 2026 Scholarly Horizon Publication. All rights reserved.